

**Statement of provenance:**

This is an author-created, un-copyedited version of an article accepted for publication in *Bioinspiration and Biomimetics*. IOP Publishing Ltd is not responsible for any errors or omissions in this version of the manuscript or any version derived from it. The Version of Record is available online at <http://dx.doi.org/10.1088/1748-3190/10/6/066004>.

# Rapid area change in pitch-up manoeuvres of small perching birds

D T Polet<sup>1</sup> and D E Rival<sup>1,2</sup>

<sup>1</sup> Department of Mechanical and Manufacturing Engineering, University of Calgary, Calgary, AB T2N 1N4, Canada

<sup>2</sup> Department of Mechanical and Materials Engineering, Queen's University, Kingston, ON K7L 3N6, Canada

E-mail: dtpolet@ucalgary.ca

1        **Abstract.** Rapid pitch-up has been highlighted as a mechanism to generate large  
2 lift and drag during landing manoeuvres. However, pitching rates had not been  
3 measured previously in perching birds, and so the direct applicability of computations  
4 and experiments to observed behaviour was not known. We measure pitch rates in  
5 a small, wild bird (the black-capped chickadee; *Poecile atricapillus*), and show that  
6 these rates are within the parameter range used in experiments. Pitching rates were  
7 characterized by the *shape change number*, a metric comparing the rate of frontal area  
8 increase to acceleration. Black-capped chickadees increase the shape change number  
9 during perching in direct proportion to their total kinetic and potential energy at the  
10 start of the manoeuvre. The linear relationship between dissipated energy and shape  
11 change number is in accordance with a simple analytical model developed for two-  
12 dimensional pitching and decelerating airfoils. Black-capped chickadees use a wing  
13 pitch-up manoeuvre during perching to dissipate energy quickly while maintaining  
14 lift and drag through rapid area change. It is suggested that similar pitch-and-  
15 decelerate manoeuvres could be used to aid in the controlled, precise landings of small  
16 manoeuvrable air vehicles.

17 *Keywords:* bird flight, perching, Micro Aerial Vehicles, rapid area change

18 Submitted to: *Bioinspir. Biomim.*

## 1. Introduction

Birds employ a diverse repertoire of unsteady manoeuvres, such as banking, braking, takeoff and landing, to navigate dense habitats and respond to gusts. Micro Aerial Vehicles (MAVs) are flying machines similar in size to small birds, designed to carry out remote sensing tasks in cluttered airspaces. Mimicking the manoeuvrability of birds, in particular the ability to land safely on small platforms, would allow these vehicles to complete their objectives effectively and efficiently. Though progress has been made in designing perching MAVs (Reich et al. 2009, Doyle et al. 2011, Moore et al. 2014), existing MAVs fall short in achieving the control, precision and speed of natural flyers in landing manoeuvres.

In order to perch, a bird must transition from a cruising speed to a standstill at landing. Perching birds simultaneously adjust their body and wing posture to become more vertical (Carruthers et al. 2007, Berg & Biewener 2010, Provini et al. 2014), as a horizontal posture reduces drag during cruising flight while an upright posture facilitates larger angles of attack for deceleration. Carruthers et al. (2007) noted that a steppe eagle would perform a *rapid pitch-up manoeuvre* during perching sequences, where the angle of attack increased continuously from near-horizontal to near-vertical. However, steady state aerodynamic analysis predicted a loss of lift at high angles of attack, due to stall effects combined with a reduction of airspeed (Carruthers et al. 2010).

Polet et al. (2015) showed that a rapidly pitching airfoil can achieve large instantaneous and time-averaged lift and drag, even while decelerating to a stop and pitching to a  $90^\circ$  angle of attack. In that study, the pitch rate was parameterized through the shape change number,  $\Xi$ . Forces increased as  $\Xi^2$  through a combination of added-mass energy transfer and vorticity generation. These results suggest that rapid area change through dynamic pitching helps generate the forces required by a perching bird to quickly decelerate and stay aloft.

Though prior works have noted body reorientation and wing pitch-up in perching birds (Carruthers et al. 2007, Berg & Biewener 2010, Provini et al. 2014), none have reported wing pitching rates in these birds or demonstrated that the resulting area change is associated with large forces on the body. We measure pitch rates in the black-capped chickadee (*Poecile atricapillus* Linnaeus 1766), a passerine abundant to North America with an average mass of about 10 g (Chaplin 1974) that will readily approach feeders at high speeds. These traits - abundance, small size, ease of attraction and speed of approach - make it an ideal candidate for studying high-performance deceleratory manoeuvres with applications to MAVs.

In the present work, we describe fast pitching during perching in the black-capped chickadee, parameterize pitch rates in terms of the shape change number, and show that black-capped chickadees alter their shape change number as the energetic demands of perching increase, implying that rapid area change through dynamic pitching is a kinematic tool that can be tuned to meet the needs of small manoeuvring air vehicles.

## 59 2. Energy dissipation through rapid area change

60 A change in angle of attack increases the frontal area of a wing. This is an example of  
 61 *rapid area change*, in which an accelerating body exhibits quick expansion or contraction  
 62 of frontal area. Weymouth & Triantafyllou (2013) showed that rapid area change is  
 63 characterized by the *shape change number*,

$$64 \quad \Xi = \frac{V^2}{aL}, \quad (1)$$

65 where  $V$  is the outward or inward velocity of area change,  $a$  is the body acceleration and  
 66  $L$  is a body length scale. Weymouth & Triantafyllou (2013) demonstrated that altering  
 67 the shape change number can dramatically modify the added mass, boundary-layer  
 68 vorticity and forces on a body.

69 These arguments were extended by Polet et al. (2015) to a two-dimensional  
 70 pitching airfoil decelerating from initial velocity  $U_0$  to a halt. Substitution of kinematic  
 71 parameters into equation (1) revealed that

$$72 \quad \Xi = \frac{V}{U_0}, \quad (2)$$

73 showing that the shape change number in their case compares the change in frontal area  
 74 relative to a characteristic change in forward velocity. As the metric shown in equation  
 75 (2) was constructed in two-dimensional space, it requires some modification to be applied  
 76 to a three-dimensional perching bird. We derive an analogous shape change number in  
 77 §4.2, after establishing the characteristic perching behaviour within *P. atricapillus*.

78 As rapid area change is an effective means to shed energy, we expect a relationship  
 79 between the shape change number used by birds and the energetic demands of a perching  
 80 manoeuvre. Once a bird has perched successfully, its kinetic and gravitational potential  
 81 energy relative to the perch are both zero. The total change in energy is therefore

$$82 \quad \Delta E = mg\Delta z + \frac{1}{2}mU_0^2, \quad (3)$$

83 where  $m$  is the bird's mass,  $g$  is the acceleration due to gravity,  $\Delta z$  is the height of  
 84 the bird's center of mass (CoM) relative to the perch and  $U_0$  the initial speed of its  
 85 CoM. In principle, any amount of energy could be dissipated with the smallest force,  
 86 given sufficient time. In practice, however, a bird needs to stay airborne until it lands.  
 87 Slow deceleration requires longer periods of sustained lift, costing metabolic energy. A  
 88 fast pitch-up quickly dissipates energy through rapid area change while simultaneously  
 89 producing enough lift to remain airborne.

90 Some energetic dissipation comes through the legs at touchdown, but the majority is  
 91 dissipated aerodynamically (Provini et al. 2014). The total energy absorbed by the legs  
 92 is limited by risk of injury, and so must be capped at a maximum value. Assuming that  
 93 energetic absorption of the legs is constant regardless of the total energetic dissipation  
 94 in perching, then the total energy dissipated aerodynamically grows in proportion to  
 95 the change in energy of perching according to equation (3).

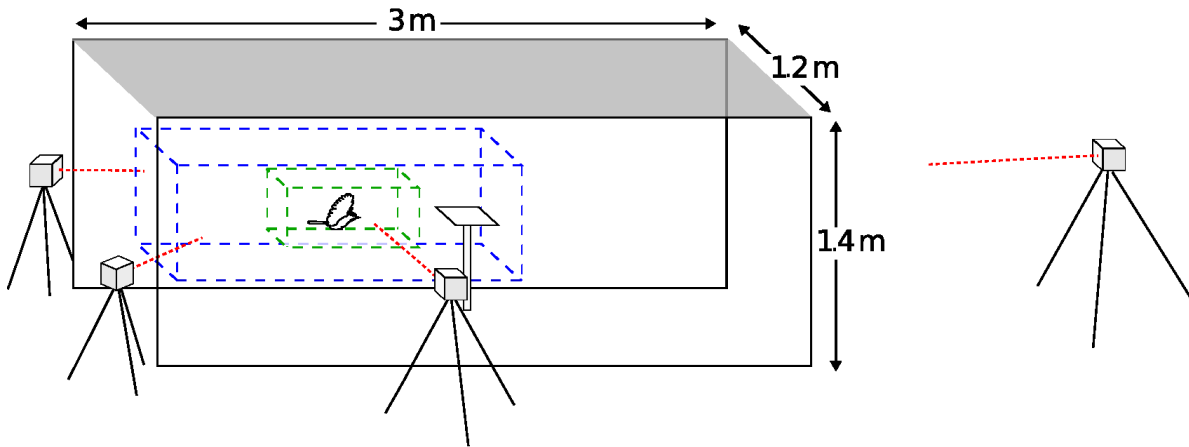


Figure 1: A diagram of the setup used in data collection. A feeder was placed at the center of an enclosure, which was open at two ends. Four cameras were positioned around the enclosure, forming two reconstruction volumes: a smaller volume for improved resolution of the pitch-up manoeuvre (green) and a larger volume to capture the entire perching sequence (blue).

96 Polet et al. (2015) showed that a pitching and decelerating airfoil produces drag  
 97 as  $D \propto \Xi^2$ , while the translational distance scaled as  $d \propto 1/\Xi$ , due to higher rates of  
 98 deceleration at higher  $\Xi$ . The total energy dissipated in such a manoeuvre scales as

$$99 \quad \Delta E \propto dD \propto \Xi. \quad (4)$$

100 Therefore, as a first approximation we expect the shape change number used by these  
 101 small birds to increase linearly with the energetic requirements of perching manoeuvres.  
 102 Predicting the slope and intercept of the proportionality (4) would require knowledge of  
 103 the maximum muscular power output and efficiency, moment of inertia about the wing  
 104 pitch axis and other biological data not available for this species. However, observing  
 105 the relationship (4) would support the hypothesis that chickadees employ rapid area  
 106 change through dynamic pitching during perching manoeuvres.

### 107 3. Experimental setup

108 A rectangular enclosure, 3 m long, 1.2 m wide and 1.4 m high was built to encourage  
 109 birds to approach from a consistent direction (figure 1). Two sheets of white polyethylene  
 110 were attached to the long sides, and two layers of 2.5 cm hexagonal wire mesh were fixed  
 111 on the upper surface. A plastic tray feeder was set 0.9 m above the ground in the center  
 112 of the enclosure, and filled with commercially available birdseed. The two smaller faces  
 113 on opposite sides of the enclosure were left open. As Green & Cheng (1998) showed  
 114 that birds will manoeuvre differently to land on a novel perch, filming began 11 days  
 115 after the feeder was placed and five days after the enclosure was finished, allowing the  
 116 birds time to acclimate to the setup.

Four Casio EX-ZR700 high-speed cameras were arranged around the enclosure to allow multiple views of perching sequences. The cameras recorded  $1224 \times 160$  pixel colour images at 480 frames per second in 13 minute intervals while birds flew to the perch freely. Shutter speed was selected automatically by internal camera software, within the range 1/500-1/10000 s. Subjects were lit using natural light on sunny days. Camera frame offsets were calculated based on an LED that flashed at the start of each filming sequence. A 10 cm calibration wand was waved through the reconstruction volume, and camera positions were calibrated using the Sparse Bundle Adjustment algorithm packaged in the MATLAB<sup>TM</sup> script *easyWand5* (Theriault et al. 2014). The reference frame was aligned to gravity by measuring the acceleration of an object falling through the reconstruction volume. Gravitational acceleration was estimated as  $95 \pm 5\%$  (mean  $\pm$  Std) of the expected value of  $9.8 \text{ m/s}^2$ . Calibration reconstruction error was estimated as 1 mm, based on the standard deviation of the wand length for all wand images, and synchronization error was estimated as  $\pm 1 \text{ ms}$ .

Over 30 perching sequences were filmed, however only 11 were deemed acceptable for analysis. The remainder were rejected due to the subject being out of frame in a camera at a critical time, not approaching through the left opening in figure 1, or if irremediable synchronization errors were detected. The acceptable sequences were digitized manually using the MATLAB<sup>TM</sup> script *DLTdv5*, written by Hedrick (2008). Details of the digitized body parts can be found in figure 2. Averaging across all trials, the direct linear transform root-mean-square-error computed by *DLTdv5* was 0.75 pixels for the beak and 1.2 pixels for the wingtip. These are the two points that were respectively the most and least clear in the videos, representing an upper and lower bound on digitization precision. After digitization, position data was processed using custom MATLAB<sup>TM</sup> scripts. Three-dimensional kinematic position data was smoothed with a second-order low-pass Butterworth filter with 50 Hz cutoff. Velocities and accelerations were computed using two-sided finite difference schemes:

$$\mathbf{u}_i = (\mathbf{x}_{i-2} - 8\mathbf{x}_{i-1} + 8\mathbf{x}_{i+1} - \mathbf{x}_{i+2}) / (12\Delta t), \quad (5)$$

$$\mathbf{a}_i = (-\mathbf{x}_{i-2} + 16\mathbf{x}_{i-1} - 30\mathbf{x}_i + 16\mathbf{x}_{i+1} - \mathbf{x}_{i+2}) / (12\Delta t^2), \quad (6)$$

where  $\mathbf{x}$ ,  $\mathbf{u}$  and  $\mathbf{a}$  refer to position, velocity and acceleration vectors, respectively, and  $\Delta t$  is the time increment between frames.

The centre of mass (CoM) was taken as the average position between the tip of the tail coverts and the base of the beak (figure 2). The tip of the tail coverts was used because it was relatively easy to distinguish in all trials. However, as both tail coverts and head are mobile relative to the CoM, artifacts in acceleration can appear as the bird adjusts its body orientation. To compensate for these artifacts in calculating instantaneous acceleration of the CoM, the true rump location (point 2b in figure 2) was digitized for one trial where it could be distinguished easily. However, movement of the head can still induce artifacts of CoM acceleration, and these will be noted where they appear in the results.

We estimated the bird's initial total energy as described in equation (3). As the

156 mass of each bird was not measured, we assumed a simple geometric scaling of body  
 157 length to mass ( $m \propto \mathcal{L}^3$ ). To attain the correct units of mass in equation (3),  $\mathcal{L}^3$  was  
 158 multiplied by the arbitrary density 1000 kg/m<sup>3</sup>, which is considered a reasonable first  
 159 estimate. Note that the precise density linking length to mass is not required to test  
 160 the proportionality expressed in equation (4) if  $m \propto \mathcal{L}^3$  is assumed. Body length was  
 161 taken as the mean distance between beak and rump tip from the end of the ballistic  
 162 phase ( $t_0$ ; see figure 2 and §4.1) up to the first complete wrist extension ( $t_1$ ; figure 2).  
 163 The birds were all of similar sizes; the average body length was 7 cm, with a range of  
 164 1 cm (N = 11).

165 Similarly,  $U_0$  is the average CoM speed from  $t_0$  to  $t_1$ .  $\Delta z$  is the height of the CoM  
 166 relative to the perch at  $t_1$ , and  $g$  is taken as 9.8 m/s<sup>2</sup>. Wing length was measured from  
 167 the wingtip to the shoulder, while the chord is measured from the shoulder to the tip of  
 168 the most proximal remige (figure 2).

169  $t_2$  is taken as the final frame before the wrist flexes following  $t_1$ , or, in the single  
 170 case where the wing tip could not be distinguished up to a minimum of two frames  
 171 after wrist flexion, as the final frame where velocity could be calculated according to  
 172 equation (5). The frame rate allowed digitization of 8 time steps on average (minimum  
 173 of 5, maximum of 13) between  $t_1$  and  $t_2$ . The wing was also digitized for a minimum of  
 174 two additional time steps both before  $t_1$  and after  $t_2$ . As the wings appear to be moving  
 175 symmetrically and yaw is not observed during the manoeuvre of interest (see §4.2), we  
 176 measured the kinematics of the right wing only.

177 The angle of attack was approximated as the wing angle relative to the plane whose  
 178 normal is  $\mathbf{z}'$  (figure 2), defined as  $\mathbf{z}' \equiv \mathbf{x}' \times \mathbf{z} \times \mathbf{x}'$ , where  $\mathbf{x}'$  denotes the displacement  
 179 vector of the center of mass from  $t_1$  to  $t_2$  and  $\mathbf{z}$  is the vertical. In the present study,  
 180 we exclusively use the proximal remige to measure wing angle; however the angle of  
 181 attack may change along the wing length. Manually digitizing the required number  
 182 of data points to measure angle of attack across the wing would be impractical, and  
 183 markers could not be attached to these wild birds without increasing the invasiveness  
 184 of the study. However, we note that angles of attack along the wing length in pigeons  
 185 do not differ significantly during any given wing stroke in perching manoeuvres (Berg &  
 186 Biewener 2010), and assume that the same is true of the black-capped chickadee. Thus,  
 187 while the angle of attack at the proximal remige may not be the average angle of attack  
 188 along the wing length, it may act as a first approximation.

## 189 4. Results and discussion

190 Eleven perching sequences were analyzed from two filming sessions five days apart.  
 191 Based on these sequences, the qualitative perching behaviour of *P. atricapillus* is  
 192 described in section §4.1. A three-dimensional extension of the two-dimensional shape  
 193 change number is established in §4.2. Quantitative kinematic results are presented in  
 194 §4.3.

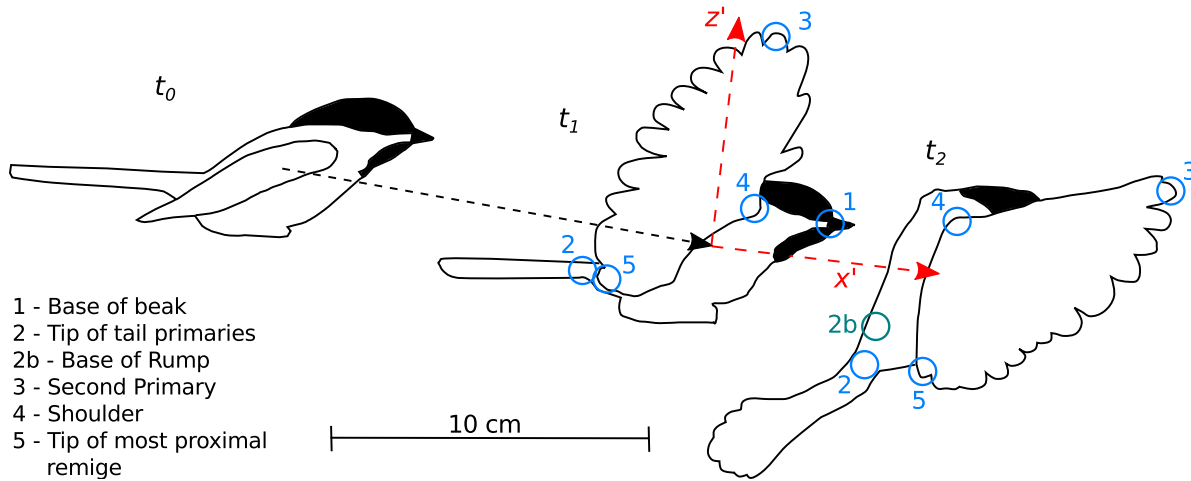


Figure 2: Outlines of a bird extracted from video frames of a single perching sequence, showing (left to right) the end of the ballistic phase ( $t_0$ ), the first frame where the wrist is fully extended ( $t_1$ ), and the final frame before the wrist flexes ( $t_2$ ). The shape change number is calculated between  $t_1$  and  $t_2$ . Note the more vertical orientation of both body and wing at  $t_2$  compared to  $t_1$ . Digitized points are shown as circles. The angle of attack was measured relative to the plane whose normal is  $\mathbf{z}'$ , defined as  $\mathbf{z}' \equiv \mathbf{x}' \times \mathbf{z} \times \mathbf{x}'$ , where  $\mathbf{x}'$  denotes the displacement vector of the centre of mass from  $t_1$  to  $t_2$  and  $\mathbf{z}$  is the vertical. The time from  $t_0$  to  $t_1$  is 38 ms and time from  $t_1$  to  $t_2$  is 23 ms in this case.

#### 195 4.1. Overview of perching behaviour in black-capped chickadees

196 Black-capped chickadees exhibit a *ballistic phase*<sup>‡</sup> before beginning deceleration (figure  
 197 2; see supplemental video S1 for a representative perching sequence, slowed 16 times).  
 198 This phase is characterized by the wings folding tightly around the body and the tail  
 199 being fully closed, with no apparent active force generation. The bird then enters a  
 200 *deceleration phase*, characterized by changes in wing and tail kinematics as well as body  
 201 orientation. At the start of this deceleration phase, the wings quickly extend to begin  
 202 the first forward power stroke. Midway through the first downstroke, the wings pitch up.  
 203 The body also shifts from a horizontal orientation to a more vertical orientation. The  
 204 tail feathers open as the body posture becomes more vertical. After the first forward  
 205 stroke, the bird performs a rearward recovery stroke and begins a sequence of between  
 206 one and four subsequent power-recovery stroke cycles before touchdown (median 2, mean  
 207 2.4, standard error 0.28,  $N = 11$ ).

208 Power strokes from the wing cause a torque about the bird's center of mass, as made  
 209 evident by the increase in body angle following the first power stroke in the deceleration  
 210 phase. However, reorientation of the body slows with further forward wing strokes when

<sup>‡</sup> Chickadees, being relatively small birds, employ flap-bounding during steady flight, a flight style where flapping and flexed-wing bounding phases alternate (Tobalske et al. 1999). The *ballistic phase* appears similar to a bounding phase, but is notable as it always occurs immediately prior to the pitch-up manoeuvre in this species.

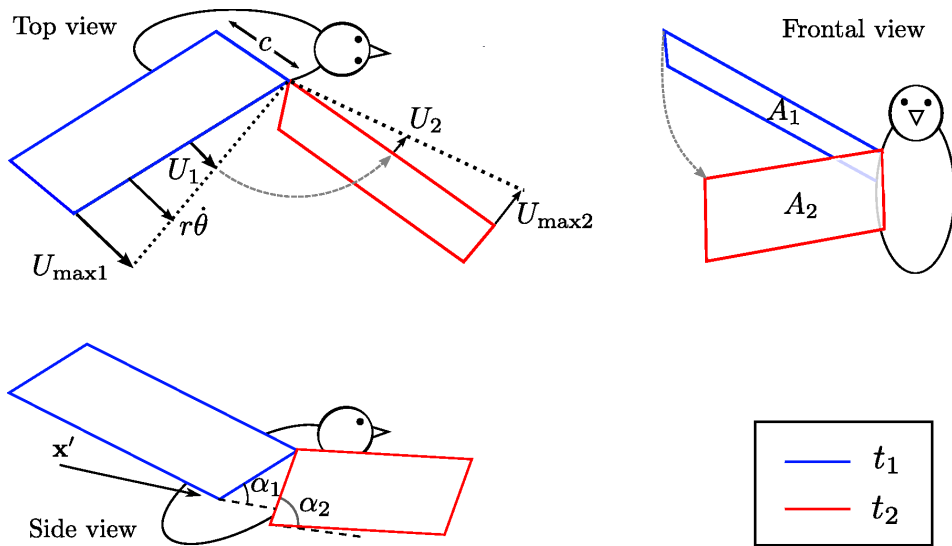


Figure 3: A cartoon showing top, frontal and side views of a bird simultaneously rotating and pitching its wings about the shoulder. Only the right wing is shown in this cartoon. The position of the wing in the bird’s frame of reference is shown at  $t_1$  and  $t_2$  (represented by blue and red, respectively), during which time the frontal area of the wing increases.

211 the tail is fully expanded. This suggests that the tail counteracts the torque produced  
 212 by the wings while also producing greater drag.

213 The mean initial flight speed of the chickadees is  $3.4 \pm 0.1$  m/s, and their landing  
 214 speed is  $1.5 \pm 0.1$  m/s (mean  $\pm$  StdErr,  $N = 11$ ). Based on their initial speed and height  
 215 relative to the perch and speed immediately before touchdown, the birds lose  $78 \pm 4\%$   
 216 of their total energy aerodynamically (mean  $\pm$  StdErr,  $N = 11$ ). This is in contrast  
 217 to 94% and 96% respectively in the larger zebra finches and diamond doves (Provini  
 218 et al. 2014), but is consistent with the notion that smaller animals tend to have more  
 219 robust legs relative to both their weight and peak locomotory stresses (Biewener 1982).  
 220 Nevertheless, chickadees dissipate the majority of their energy aerodynamically during  
 221 perching; thus, aerodynamic mechanisms remain crucial to a successful landing.

222 In black-capped chickadees, the first downstroke involves a pronounced wing pitch-  
 223 up manoeuvre, with observed pitch rates ranging between 16 and 39 rads/s. We therefore  
 224 analyzed this downstroke in detail using the smaller reconstruction volume (figure 1) to  
 225 quantify the shape change number and associated forces.

#### 226 4.2. A three-dimensional analogue to the two-dimensional shape change number

227 Here we extend the two-dimensional shape change number ( $\Xi$ ) for a pitching and  
 228 decelerating airfoil (equation 1) to an analogous metric relevant to the first perching  
 229 power stroke described in §4.1. During the first stroke, there are three ways in which  
 230 black-capped chickadees can use control surfaces to change frontal area: (1) extending  
 231 and morphing the wings as they unfold from the body, (2) expanding and pitching

the tail and (3) pitching the wings. The latter is most similar to earlier work on two-dimensional pitching airfoils, and so is most amenable to comparative analysis. The first two effects merit future study but are beyond the scope of the present work.

For black-capped chickadees, the majority of wing pitching occurs after the wings are fully extended. From the timestep where the wrist is first extended fully ( $t_1$ ) to the timestep immediately before the wrist flexes again ( $t_2$ ; see figure 2), on average the maximum change in wing length is 13% ( $\sim 1/8^{\text{th}}$ ) of the mean. The small change in wing planform shape fortuitously separates the effects of area change due to pitching from wing expansion. Therefore,  $\Xi$  is calculated between  $t_1$  and  $t_2$ . The pitch angle to the CoM translation is measured at these two points ( $\alpha_1$  and  $\alpha_2$ , respectively; figure 3). We are interested in the area change normal to the chordwise airspeed. Taking the chord length,  $c$ , and setting  $T = t_2 - t_1$ , the shape change velocity is then

$$V = \frac{c(\sin \alpha_2 - \sin \alpha_1)}{T}. \quad (7)$$

The shape change number requires a characteristic translational velocity change ( $\Delta U$ ). Between  $t_1$  and  $t_2$ , the wing performs a sweeping motion about the shoulder (figure 3). The average chordwise airspeed across the wing is approximately equal to the speed of the wing, normal to its length, at the midpoint between shoulder and wingtip (figure 3). We calculate these airspeeds at  $t_1$  and  $t_2$ , producing  $U_1$  and  $U_2$  respectively<sup>§</sup>. As the bird must perform a recovery stroke following  $t_2$ , the wings decelerate from  $t_1$  to  $t_2$  while pitching up. Thus, the analogous deceleration to a two-dimensional pitch-and-decelerate manoeuvre is  $a = \Delta U/T = (U_2 - U_1)/T$ .

Inserting these kinematic values into equation (1) and setting  $c = L$ , we arrive at

$$\Xi = \frac{V[\sin(\alpha_2) - \sin(\alpha_1)]}{\Delta U}. \quad (8)$$

Using the same parameters as Polet et al. (2015) ( $\alpha_1 = 0^\circ$ ,  $\alpha_2 = 90^\circ$ ,  $\Delta U = U_0$ ), we recover equation (2). Thus, equation (8) is analogous to the two-dimensional shape change number for a pitching and decelerating airfoil, and compares the rates of change of frontal width and sweep velocity in a pitching wing.

Note that equation (8) no longer requires a deceleration to a halt, in contrast to equation (2). Therefore, it is not necessarily true that  $d \propto 1/\Xi$  and a correction factor must be added to equation (4). Assuming constant deceleration from  $U_1$  to  $U_2$ , we can express the distance the wing travels as  $d = (U_1 + U_2)T/2$ . Using equations 7 and 8, it can be easily shown that

$$d = \frac{U_1 + U_2}{U_1 - U_2} \frac{c(\sin \alpha_2 - \sin \alpha_1)^2}{2\Xi}. \quad (9)$$

Thus, the relationship between  $\Delta E$  and  $\Xi$  becomes

$$\Delta E \propto \left( \frac{U_1 + U_2}{U_1 - U_2} c(\sin \alpha_2 - \sin \alpha_1)^2 \right) \Xi \equiv \mathcal{C}\Xi, \quad (10)$$

<sup>§</sup> Based on the average values of  $\bar{c} = 0.04$  m and  $\bar{U}_1 = 5.9$  m/s, the Reynolds number in these perching sequences is approximately  $2.4 \times 10^4$ , similar to the value of  $2.2 \times 10^4$  used by Polet et al. (2015)

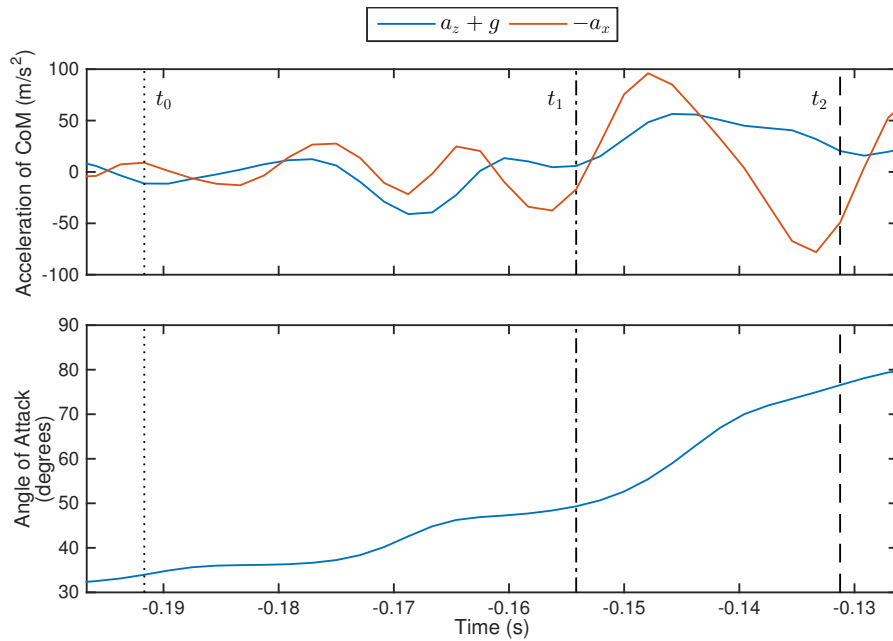


Figure 4: A representative trial, showing that black-capped chickadees exhibit relatively large center-of-mass (CoM) accelerations along with a rapid increase in angle of attack from the first moment when the wing wrist is fully extended ( $t_1$ ) to the moment where it is flexed once again ( $t_2$ ). As the CoM is measured as the midpoint of beak and rump, the peak forward acceleration near the point of arm flexion is likely an artifact due to the head remaining level while the body posture becomes more vertical (figure 2).

267 where the symbol  $\mathcal{C}$  is given to the correction factor.  $\mathcal{C}\mathcal{E}$  is proportional to the  
 268 aerodynamic energetic dissipation from area change through pitching, which we expect  
 269 to increase along with the energetic demands of a perching manoeuvre.

#### 270 4.3. Rapid pitch-up manoeuvres and area change to increase force production

271 Figure 4 shows the instantaneous CoM accelerations due to vertical and rearward forces  
 272 (roughly lift and drag) for a representative trial. Vertical lines denote  $t_0$ ,  $t_1$  and  $t_2$   
 273 as shown in figure 2. The greatest pitching occurs between  $t_1$  and  $t_2$ . A relatively  
 274 large peak in vertical and rearward acceleration occurs at the onset of the pitch-up  
 275 manoeuvre. The peak rearward acceleration is followed by a peak forward acceleration.  
 276 Since the CoM is defined as the average position of beak and rump, the peak forward  
 277 acceleration is likely an artifact of the forward rotation of the head relative to the body  
 278 (figure 2). This same rotation would also detract from the observed magnitudes of  
 279 rearward acceleration; thus, despite these artifacts figure 4 shows that the largest drag  
 280 produced between  $t_0$  to  $t_2$  occurs during the pitch-up manoeuvre when the wrists are  
 281 fully extended.

282 Figure 5a plots the shape change number according to equation (8) for individual  
 283 perching sequences against each bird's total potential and kinetic energy relative to

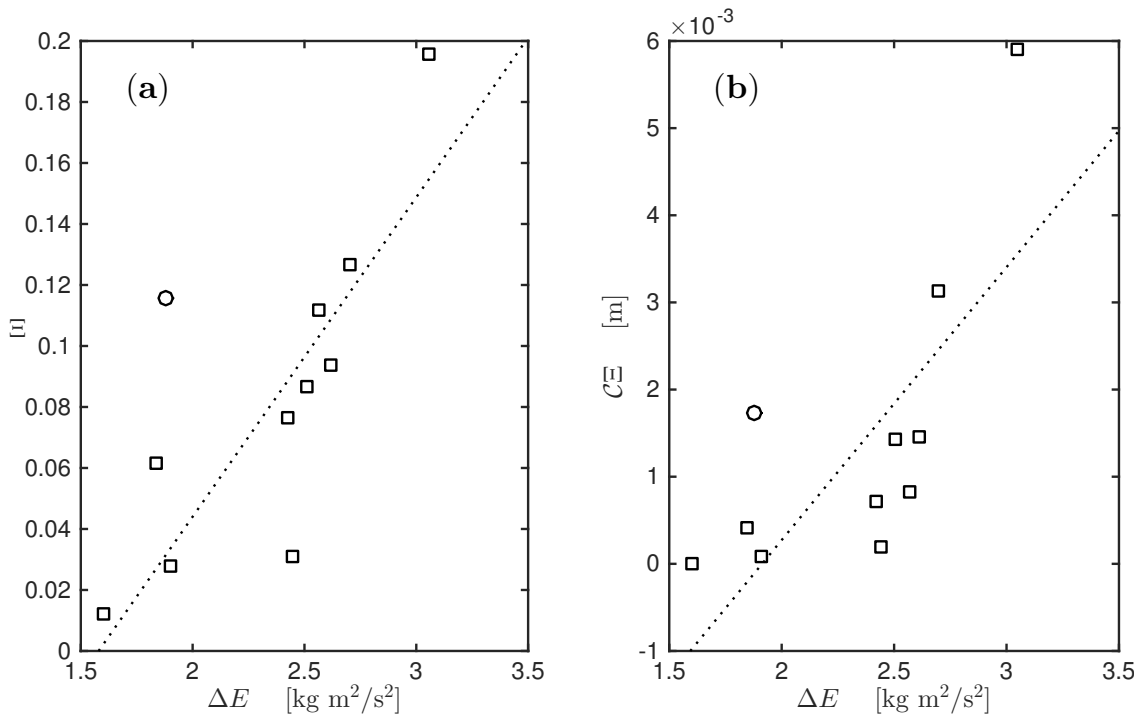


Figure 5: Black-capped chickadees choose higher shape change numbers from wing pitching as the total energetic requirements of the perching manoeuvre increase. **(a)** The linear trend observed here is consistent with predictions based on pitching and decelerating airfoils (Polet et al. 2015), without corrections for distance travelled (§4.2). In the trial denoted with a circle, the bird exhibited a different landing pattern from the others as described in the text. Excluding this outlier, the least-squares residual is shown as a dotted line ( $R^2 = 0.73$ ,  $p = 0.002$ ). **(b)** Here the shape change number is multiplied by a correction factor  $\mathcal{C}$  for the new three-dimensional metric (equation 10), and increases with energetic dissipation ( $R^2 = 0.59$ ;  $p = 0.01$ ).

284 the perch at  $t_0$ . Shape change number varies from 0.01 to 0.20, within the range  
 285 tested by Polet et al. (2015). Shape change number increases with initial kinematic  
 286 energy, supporting the hypothesis that pitch rates are tuned by small birds to the  
 287 energetic demands of the perching manoeuvre. Using all trials, the  $R^2$  value of the  
 288 linear least-squares fit is 0.54 ( $p = 0.01$ ). Of note is a single trial, denoted by a circle in  
 289 figure 5, which exhibits a much higher shape change number given its initial energy as  
 290 compared to the others. In this sequence, unlike the others, the bird slowed to a near  
 291 halt before landing, and required an extra lunge near the perch to achieve touchdown  
 292 (see supplementary video S2). It may be that this individual overestimated its energy  
 293 requirements and used a higher shape change number than needed to land smoothly.  
 294 Excluding this outlier, the  $R^2$  value is 0.73 ( $p = 0.002$ ), supporting the relationship  
 295 developed in equation (4).

296 In §4.2, it was noted that the new three-dimensional shape change metric does not  
 297 necessarily require  $d \propto 1/\Xi$ , and so a correction factor  $\mathcal{C}$  is necessary in the relationship

298 between energetic dissipation from area change and total energy change in perching.  
 299 The shape change number multiplied by this correction factor is plotted against energy  
 300 change in figure 5b. The trend remains linear overall, but with greater scatter about  
 301 central tendency. Excluding the outlier as before, the  $R^2$  value is 0.59 ( $p = 0.01$ ).

302 It may seem that spurious correlations between  $\Delta E$  and  $\Xi$  would arise due to the  
 303 CoM speed  $U_0$  being a component of the wing velocities  $U_1$  and  $U_2$ , as the former term  
 304 appears in  $\Delta E$  and the latter two terms in  $\Xi$ . However, if  $U_0 \propto U_1 - U_2$ , we would  
 305 expect a reciprocal relationship in figure 5a in the absence of a physical mechanism  
 306 linking  $\Xi$  and  $\Delta E$ . As a positive linear trend is observed instead, we conclude that the  
 307 proposed physical mechanism is indeed responsible.

308 For  $\mathcal{C}\Xi$  vs.  $\Delta E$ , a spurious correlation may arise if  $U_1 + U_2$  is proportional to  $U_0$  and  
 309  $U_1 - U_2$  is not. We therefore tested a linear model on  $\mathcal{C}\Xi/(U_1 + U_2)$  vs.  $\Delta E$ , eliminating  
 310  $U_1 + U_2$  in the response variable, and found  $R^2 = 0.65$  and  $p = 0.005$  ( $N = 10$ ). Thus,  
 311 it is unlikely that the dependence of  $U_1 + U_2$  on  $U_0$  is responsible for the correlation  
 312 observed between  $\mathcal{C}\Xi$  and  $\Delta E$ , and rather that the correlation arises because energetic  
 313 dissipation due to pitch-up is proportional to total energy change during perching.

314 Because no specimens were captured and marked, and morphological differences  
 315 between individual chickadees are slight, we could not determine if the same individuals  
 316 were filmed multiple times. For the present study, we assume that individual biases were  
 317 minor, and note that the twofold range of  $\Delta E$  and tenfold range of  $\Xi$  provides sufficient  
 318 variation to test the dependence of shape change number on energetic dissipation in  
 319 this sample. A future study could capture and mark individuals to test if individual  
 320 preferences play an important role in the strategies employed; however, such a study  
 321 would be more invasive.

322 In §2 it was assumed that energetic absorption from the legs would be constant  
 323 regardless of total energy change in perching. In reality, birds may reduce loading in the  
 324 legs for less energetic perching manoeuvres, and gradually increase the loading for more  
 325 energetic manoeuvres up to a particular limit determined by risk of injury. At this point,  
 326 any additional energy change is exclusively absorbed aerodynamically. Accordingly, in  
 327 figure 5b the energetic dissipation through area change ( $\mathcal{C}\Xi$ ) increases slowly as the  
 328 total energy change during perching ( $\Delta E$ ) increases, up to approximately  $\Delta E = 2.5$  J,  
 329 at which point further increase in the energy change results in a substantial increase in  
 330 the energetic dissipation from area change ( $\mathcal{C}\Xi$ ). A follow-up study could use a perch  
 331 with a built-in force transducer, as used by Bonser & Rayner (1996) and Provini et al.  
 332 (2014), to see how energy absorption through perch collision changes with the energetics  
 333 of a perching manoeuvre.

334 Birds smaller than 30 g with short, rounded wings seldom glide, and must  
 335 instead flap frequently to remain airborne (Tobalske 2007). Accordingly, black-capped  
 336 chickadees perform a rapid pitch-up manoeuvre during a power stroke, rather than  
 337 during a glide as observed in a steppe eagle (Carruthers et al. 2007). Performing wing  
 338 pitch-up at the beginning of the deceleration phase begins the transition to the correct  
 339 posture for landing while dissipating a large amount of energy. This facilitates slower

340 speeds as the bird approaches the perch and precise control becomes critical, enabling  
341 these birds to decelerate on average from 47 body lengths per second to a halt in less  
342 than 0.3 seconds.

343 The acceleration artifacts from head rotation in this dataset prohibits direct  
344 comparison of shape change number and instantaneous acceleration during the pitch-  
345 up manoeuvre. Future work could achieve better CoM estimates using markers on  
346 captive birds, but this is not an option for wild specimens. While figure 5 shows a  
347 strong relationship between shape change number and energetic demands, the exact  
348 nature of this relationship should be taken cautiously. Mass could only be estimated  
349 as a proportion to length raised to the third power and could not be measured directly.  
350 Future studies could implement a weigh scale into the perch itself, enabling accurate  
351 measurements of mass once the bird has landed. This would then allow a more precise  
352 measure of the exact relationship between area change and energetic demands.

353 The relationship between pitch rates and energetic dissipation demonstrated in  
354 figure 5 suggests a simple, first-order algorithm that could be employed by MAVs during  
355 perching manoeuvres: (1) determine the required energy to be dissipated before landing,  
356 (2) employ a pitch-up manoeuvre where the shape change number is in proportion to  
357 this energy. The slope and intercept of this relationship may well depend on particulars  
358 of the shape and size of the aircraft employed. However, the linear relationship between  
359 shape change number and energetic dissipation suggests that the slope could be easily  
360 calibrated, and the appropriate pitch speed could be readily retrieved during actual  
361 perching manoeuvres.

362 The large peak in lift and drag at the onset of pitching and the choice of larger shape  
363 change numbers for more energetic perching manoeuvres support the hypothesis that  
364 black-capped chickadees use rapid area change through dynamic pitching to generate  
365 large forces for a successful landing. Though high angles of attack can be associated  
366 with a loss of lift and control in steady-state flight, black-capped chickadees appear to  
367 use a rapid pitch-up manoeuvre— and thus unsteady aerodynamic trickery— to dissipate  
368 large amounts of energy dynamically.

## 369 5. Conclusions

370 Birds must be able to dissipate a large amount of energy during landing, but slow  
371 deceleration demands longer periods of sustained lift, costing metabolic energy. Rapid  
372 pitch-up manoeuvres have been linked to rapid energy dissipation in laboratory  
373 experiments on perching airfoils, but pitch rates had not been measured for these  
374 manoeuvres in birds. We observed that black-capped chickadees perform a pitch-up  
375 manoeuvre during the first deceleratory stroke. This initiates transition to the correct  
376 landing posture while also generating large lift and drag. Pitching rates during this  
377 power stroke were characterized by the *shape change number*, a metric comparing the  
378 rate of frontal area increase to wing acceleration. The shape change number was  
379 constructed to be appropriate for the manoeuvres employed by black-capped chickadees

380 while being analogous to the parameter used by Polet et al. (2015), who revealed that  
381 forces increase quadratically with the shape change number in a perching airfoil. We  
382 expected and observed black-capped chickadees to choose larger shape change numbers  
383 as the energetic demands of the manoeuvre increased. The relationship between shape  
384 change number and the total energy change in perching is generally linear, in accordance  
385 with simple analytical arguments. These small birds employ rapid-area change through  
386 pitching to enable extraordinary manoeuvrability.

## 387 Acknowledgements

388 The authors wish to thank the Natural Sciences and Engineering Research Council of  
389 Canada and Alberta Innovates Technology Futures for financial support.

## 390 References

- 391 Berg, A. & Biewener, A. (2010). Wing and body kinematics of takeoff and landing flight in the pigeon  
392 (*Columbia livia*), *Journal of Experimental Biology* **213**: 1651–1658.
- 393 Biewener, A. A. (1982). Bone strength in small mammals and bipedal birds: do safety factors change  
394 with body size?, *Journal of Experimental Biology* **98**(1): 289–301.
- 395 Bonser, R. & Rayner, J. (1996). Measuring leg thrust forces in the common starling, *Journal of*  
396 *Experimental Biology* **199**(2): 435–439.
- 397 Carruthers, A. C., Thomas, A. L. R. & Taylor, G. K. (2007). Automatic aeroelastic devices in the  
398 wings of a steppe eagle *Aquila nipalensis*, *Journal of Experimental Biology* **210**(23): 4136–4149.  
399 **URL:** <http://jeb.biologists.org/content/210/23/4136.abstract>
- 400 Carruthers, A. C., Thomas, A. L. R., Walker, S. M. & Taylor, G. K. (2010). Mechanics  
401 and aerodynamics of perching manoeuvres in a large bird of prey, *Aeronautical Journal*  
402 **114**(1161): 673–680.
- 403 Chaplin, S. B. (1974). Daily energetics of the black-capped chickadee, *Parus atricapillus*, in winter,  
404 *Journal of Comparative Physiology* **89**(4): 321–330.
- 405 Doyle, C., Bird, J., Isom, T., Johnson, C., Kallman, J., Simpson, J., King, R., Abbott, J. & Minor,  
406 M. (2011). Avian-inspired passive perching mechanism for robotic rotorcraft, *Intelligent Robots*  
407 *and Systems (IROS), 2011 IEEE/RSJ International Conference on*, pp. 4975–4980.
- 408 Green, P. R. & Cheng, P. (1998). Variation in kinematics and dynamics of the landing flights of pigeons  
409 on a novel perch, *Journal of Experimental Biology* **201**(24): 3309–3316.
- 410 Hedrick, T. L. (2008). Software techniques for two- and three-dimensional kinematic measurements of  
411 biological and biomimetic systems, *Bioinspiration & Biomimetics* **3**(3): 034001.
- 412 Moore, J., Cory, R. & Tedrake, R. (2014). Robust post-stall perching with a simple fixed-wing glider  
413 using lqr-trees, *Bioinspiration & Biomimetics* **9**(2): 025013.  
414 **URL:** <http://stacks.iop.org/1748-3190/9/i=2/a=025013>
- 415 Polet, D. T., Rival, D. E. & Weymouth, G. D. (2015). Unsteady dynamics of rapid perching  
416 manoeuvres, *Journal of Fluid Mechanics* **767**: 323–341.
- 417 Provini, P., Tobalske, B. W., Crandell, K. E. & Abourachid, A. (2014). Transition from wing to leg  
418 forces during landing in birds, *Journal of Experimental Biology* **217**: 2659–2666.  
419 **URL:** <http://jeb.biologists.org/content/early/2014/05/08/jeb.104588.abstract>
- 420 Reich, G., Wojnar, O. & Albertani, R. (2009). Aerodynamic performance of a notional perching  
421 MAV design, *47th AIAA Aerospace Sciences Meeting*, American Institute of Aeronautics and  
422 Astronautics, pp. 2009–63.  
423 **URL:** <http://dx.doi.org/10.2514/6.2009-63>

- 424 Theriault, D. H., Fuller, N. W., Jackson, B. E., Bluhm, E., Evangelista, D., Wu, Z., Betke, M. &  
425 Hedrick, T. L. (2014). A protocol and calibration method for accurate multi-camera field  
426 videography, *Journal of Experimental Biology* **217**(11): 1843–1848.
- 427 Tobalske, B., Peacock, W. & Dial, K. (1999). Kinematics of flap-bounding flight in the zebra finch  
428 over a wide range of speeds, *Journal of Experimental Biology* **202**(13): 1725–1739.  
429 **URL:** <http://jeb.biologists.org/content/202/13/1725.abstract>
- 430 Tobalske, B. W. (2007). Biomechanics of bird flight, *Journal of Experimental Biology* **210**(18): 3135–  
431 3146.
- 432 Weymouth, G. & Triantafyllou, M. S. (2013). Ultra-fast escape of a deformable jet-propelled body,  
433 *Journal of Fluid Mechanics* **721**: 367–385.